
Article:
Bougouffa, S. and Babiker, M. orcid.org/0000-0003-0659-5247 (2023) Absorption of hybrid fibre modes by Cs atoms in quadrupole transitions. Journal of Physics B: Atomic, Molecular and Optical Physics. 215002. ISSN 1361-6455

https://doi.org/10.1088/1361-6455/acfd71

Absorption of hybrid fibre modes by Cs atoms in quadrupole transitions

OPEN ACCESS
IOP Publishing
Journal of Physics B: Atomic, Molecular and Optical Physics
J. Phys. B: At. Mol. Opt. Phys. **56** (2023) 215002 (12pp)
https://doi.org/10.1088/1361-6455/acfd71

Absorption of hybrid fibre modes by Cs atoms in quadrupole transitions

S Bougouffa[1] **and M Babiker**[2,*]

[1] Department of Physics, College of Science, Imam Mohammad Ibn Saud Islamic University (IMSIU), PO Box 90950, Riyadh 11623, Saudi Arabia
[2] Department of Physics, University of York, Heslington, York YO10 5DD, United Kingdom

E-mail: m.babiker@york.ac.uk

Received 8 March 2023, revised 14 September 2023
Accepted for publication 26 September 2023
Published 17 October 2023

Abstract

We evaluate the rate of the absorption of an optical nanofibre mode by a Cs atom in an electric quadrupole transition. With the Cs atom localised near the outer surface of the optical nano-fibre, an interaction occurs between the atomic quadrupole tensor components and the gradients of the vector components of the electric field of a hybrid fibre mode. The absorption rate is evaluated as a function of the radial position of the atom from the fibre axis, assuming a specific value of the laser power and we use experimentally accessible parameters. We find that the absorption of the hybrid modes by the Cs atom decreases as the atom recedes away from the fibre axis and it formally vanishes at sufficiently large radial distances. Close to the fibre, however, the absorption rate for the input power chosen can be two orders of magnitude larger than the quadrupole de-excitation rate despite the moderate power used.

Keywords: quadrupole interaction, optical fibre modes, absorption rate

(Some figures may appear in colour only in the online journal)

1. Introduction

It is well-known that both the rates of emission and absorption of the light by a two-level atom are modified when the atom is localised near the surface of a material object. The presence of the material object modifies the electromagnetic fields with which the two-level atom interacts, leading to significant changes of the rates of emission and absorption [1–11]. For example, if the atomic transition is dipole-active and the atom is localised between two conductor slabs separated by a sub-wavelength distance, then the emission process can be totally suppressed and so, in the absence of any other influences, the atom remains excited indefinitely.

The most widely considered two-level system in such problems is assumed to have a dipole-active transition, but atomic systems can have transitions between their energy levels which are dipole-forbidden, but quadrupole-allowed, as in the case of Cs, Na, and Rb. Recent studies by both theory and experiment have focused on such atoms [12–18]. Quadrupole transitions are, of course, normally much weaker than dipole transitions and often their observation requires intense input laser light. However, it is possible to circumvent the use of intense input light and seek to create situations where the fields are sufficiently intense in well-defined regions of space even though the input power is not high. Indeed the region close to a material surface can have a high electromagnetic density of states with the energy concentrated in a tiny volume near the surface.

In this paper we are concerned with the quadrupole interaction of a two-level atom with the electromagnetic fields outside an optical fibre as the material object. There are a number of reasons why such a physical scenario is novel. Firstly there is the experimental possibility of considering an ultra-thin optical fibre which can be immersed in a cold dilute atomic

* Author to whom any correspondence should be addressed.

gas as in the recent experiment by Ray *et al* [15]. Secondly, the guided modes of the optical nano-fibre introduce new effects due to the twisting of the helical wave fronts associated with the phase function $e^{ip\ell\phi}$ with $p=\pm1$ and ℓ a positive integer. Thirdly the propagation of the electromagnetic fields in an optical fibre is characterised by a chirality in the sense that it distinguishes between axial propagation along the $+z$ and the $-z$ axes. We seek to determine how these features impact on the quadrupole interaction of the nano-fibre modes with the two-level atom which is localised outside its surface. We focus on the absorption process involving the quadrupole transition of a Cs atom which is assumed to be localised in the vicinity of the fibre surface. The aim is to evaluate the upward transition rate for a specific power of the input laser needed to excite the fibre mode.

Figure 1 schematically presents the 'optical fibre + atom' system where the two-level atom of transition frequency ω_a is situated outside the fibre at $\mathbf{R}=(\rho,0,0)$ where $\rho\geqslant a$, with a the radius. This problem is essentially a two-centre problem with two sets of coordinate systems separated by the radial vector $\boldsymbol{\rho}$. We assume that the fibre mode propagating along its axis in the $+z$-direction has a z component of angular momentum denoted by $\mathcal{L}_z^{\rm fibre}$, say, relative to the fibre frame of reference. However, relative to the atomic frame the z-component of the angular momentum is $\mathcal{L}_z^{\rm atom}$ which is given by

$$\mathcal{L}_z^{\rm atom}=\mathcal{L}_z^{\rm fibre}-[\rho\times\bar{\boldsymbol{\pi}}]_z=\mathcal{L}_z^{\rm fibre}-\frac{1}{2}\varepsilon_0\rho S_\varphi \tag{1}$$

where we have defined $\bar{\boldsymbol{\pi}}=\frac{1}{c^2}\mathbf{S}$ as the linear momentum density, $\mathbf{S}=\frac{1}{2}\Re[\mathbf{E}^*\times\mathbf{H}]$ the Poynting vector with $\mathbf{E}$ and $\mathbf{H}$, the electric and magnetic fields of the fibre mode. On applying the results of the analysis to a particular fibre mode and a particular atomic transition we have to determine whether the second term is sufficiently small to write

$$\mathcal{L}_z^{\rm atom}\approx\mathcal{L}_z^{\rm fibre} \tag{2}$$

which means that for interactions at the atomic position the optical angular momentum of the mode differs very little from that relative to the fibre frame of reference. In appendix B we evaluate the cylindrical components of the Poynting vector of the specific fibre mode and conclude that the azimuthal component of the Poynting vector, S_φ, is small in the region outside the fibre and the near equality in equation (2) is reasonably well justified for the parameters chosen. The above argument was put forward by Berry [19] in the context of free space optical vortex modes, but here we had to check and confirm its validity for fibre modes.

The flow of this paper is as follows. In section 2 we describe the relevant hybrid modes of the optical fibre and we focus on the Cs quadrupole transitions $|L=0,m_l=0\rangle\rightarrow|L=2,m_l'\rangle$ where $m_l'=0,\pm1,\pm2$. In section 3 we present the general formalism of the emitter as a two-level system interacting with an external optical field through an electric quadrupole transition. In section 4 analytical expressions are derived for the quadrupole Rabi frequency associated with the absorption of the light in a quadrupole transition of a Caesium atom. Section 5 is concerned with the absorption process when the atom interacts with the optical fibre field at near-resonance, with the aim of evaluating the absorption rate. The model treats the atom as a two-level system and applies the Fermi Golden rule involving the density of states with appropriate use of the transition selection rules. In presenting the rate of transition formalism we describe the density of the continuum final states as a Lorentzian function representing the upper atomic level as an energy band of width $\hbar\gamma$ where γ^{-1} is the free space lifetime of the upper state involved in the quadrupole transition. We adopt experimentally accessible parameters to evaluate the magnitude of the absorption rate. In section 6 we summarise and outline the main conclusions of this paper.

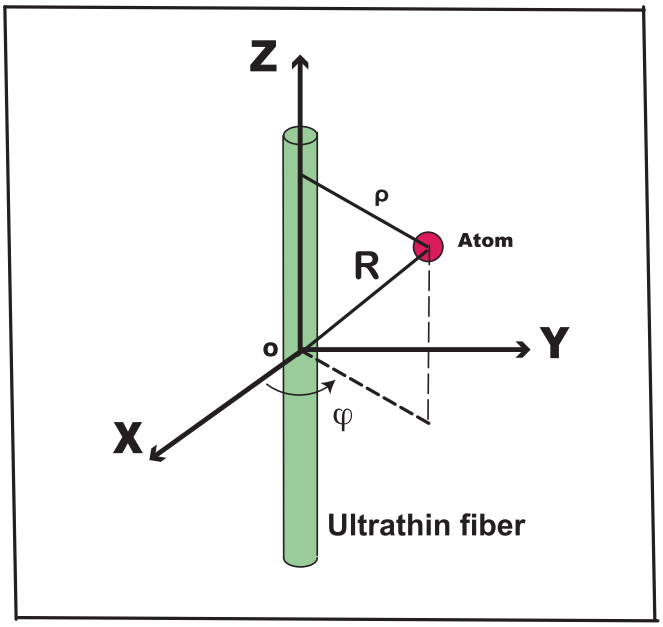

Figure 1. An atom, as a two-level system, localised at the position vector $\mathbf{R}$ in the vicinity of the optical fibre where use is made of both the Cartesian coordinate system $\mathbf{R}=\{X,Y,Z\}$ and cylindrical polar coordinates $\mathbf{R}=(\rho,\varphi,Z)$. The refractive indices in the core n_1 and in the cladding regions n_2 are both constants.

2. Hybrid nano-fibre modes

The electromagnetic fields with which the emitter interacts are those in the vicinity of the surface of a nano-fibre in the form of a long circular solid cylinder as shown in figure 1 with the fibre surrounded by a homogeneous medium (cladding). The refractive indices in the core region, n_1, and in the cladding region, n_2, are both assumed to be constants. The theory of fibre modes is described in detail in [20–22], so only a brief mention of the modes and more details pertaining to the hybrid modes are presented here.

Since the refractive indices in the core and the cladding regions are both constants the fibre can only support guided

modes. Thus the types of guided modes that can be excited in the optical fibre are quasi-circularly polarised hybrid modes (HE or EH), transverse electric modes (TE), and transverse magnetic modes (TM). For ease of notation, the fibre guided modes of frequency ω and axial wavenumber k will now be labelled by the index $\alpha = \{\omega, C, s, p\}$, with the label $C = \mathrm{HE}_{\ell m}, \mathrm{EH}_{\ell m}, \mathrm{TE}_{0m}$, or TM_{0m} representing the mode kind of integer $\ell = 0, 1, 2, \ldots$ and $m = 1, 2, \ldots$, with ℓ the winding number and m the radial index, respectively. The index $s = -1$ or $+1$ denotes the backward or forward propagation along the fibre axis z, and $p = \pm 1$ denotes the polarisation index. As pointed out earlier, we adopt cylindrical polar coordinates to represent the position vector variable of the centre of mass $\mathbf{R}$ of the atom, so that $\mathbf{R} = (\rho, \varphi, Z)$. We write for the electric field of a guided mode

$$\mathbf{E}(\mathbf{R}, t) = \boldsymbol{\mathcal{E}}(\rho)\, \mathrm{e}^{i\theta^{\alpha}} \mathrm{e}^{-i\omega t} + \mathrm{c.c.} \tag{3}$$

where $\theta^{\alpha} = s\beta Z + p\ell\varphi$ is the phase function with β the propagation constant. In most standard treatments of the guided modes of an optical fibre the vector amplitude function $\boldsymbol{\mathcal{E}}(\rho)$ is normally derived using cylindrical polar coordinates. It has three components, namely radial, azimuthal, and axial components, and is written as $(\mathcal{E}_{\rho}, \mathcal{E}_{\varphi}, \mathcal{E}_{Z})$. The quasi-circularly polarised hybrid mode [13, 20–23] is the type of mode of particular importance here.

2.1. Quasi-circularly polarised hybrid modes

For integer $\ell > 0$ we have the quasi-circularly polarised hybrid modes $C = \{\mathrm{HE}_{\ell m}$ or $\mathrm{EH}_{\ell m}\}$ and are defined both inside the fibre $(\rho < a)$ and outside it $(\rho > a)$. The components of the electric field inside the fibre $\rho < a$ are as follows

$$\begin{aligned}
\mathcal{E}_{\rho} &= i\mathcal{N}\frac{\beta}{2\mu}\left[(1-\xi)J_{\ell-1}(\mu\rho) - (1+\xi)J_{\ell+1}(\mu\rho)\right], \\
\mathcal{E}_{\varphi} &= -\mathcal{N}\frac{\beta}{2\mu}\left[(1-\xi)J_{\ell-1}(\mu\rho) + (1+\xi)J_{\ell+1}(\mu\rho)\right], \\
\mathcal{E}_{Z} &= \mathcal{N}J_{\ell}(\mu\rho),
\end{aligned} \tag{4}$$

and, for $\rho > a$,

$$\begin{aligned}
\mathcal{E}_{\rho} &= i\mathcal{N}\frac{\beta}{2\nu}\frac{J_{\ell}(\mu a)}{K_{\ell}(\nu a)}\left[(1-\xi)K_{\ell-1}(\nu\rho) + (1+\xi)K_{\ell+1}(\nu\rho)\right], \\
\mathcal{E}_{\varphi} &= -\mathcal{N}\frac{\beta}{2\nu}\frac{J_{\ell}(\mu a)}{K_{\ell}(\nu a)}\left[(1-\xi)K_{\ell-1}(\nu\rho) - (1+\xi)K_{\ell+1}(\nu\rho)\right], \\
\mathcal{E}_{Z} &= \mathcal{N}\frac{J_{\ell}(\mu a)}{K_{\ell}(\nu a)}K_{\ell}(\nu\rho).
\end{aligned} \tag{5}$$

where ξ is a system parameter, defined as

$$\xi = l\left(\frac{1}{\mu^2 a^2} + \frac{1}{\nu^2 a^2}\right)\left[\frac{J'_{\ell}(\mu a)}{\mu a J_{\ell}(\mu a)} + \frac{K'_{\ell}(\nu a)}{\nu a K_{\ell}(\nu a)}\right]^{-1}, \tag{6}$$

where the prime stands for the total derivative. In the above field components, $\mu = (n_1^2 k^2 - \beta^2)^{1/2}$ is the wave number associated with the radial variation of the field inside the fibre, and $\nu = (\beta^2 - n_2^2 k^2)^{1/2}$ is associated with the spatial decay of the field amplitude radially outside the fibre. The functions J_n and K_n, with n integer, are Bessel functions of the first kind and modified Bessel functions of the second kind, respectively. Finally, $\mathcal{N}$ is the overall constant which is determined in terms of the power $\mathcal{P}$ of the field. The evaluation of $|\mathcal{N}|$ is described in appendix A in which we find $|\mathcal{N}|$ is given by

$$|\mathcal{N}|^2 = \frac{\mathcal{P}}{\mathcal{I}_{H1} + \mathcal{I}_{H2}} \tag{7}$$

where for the $\mathcal{I}_{H1}$ and $\mathcal{I}_{H2}$ are the integrals appearing in the appendix as in equations (A.6) and (A.7) and are to be evaluated numerically.

The set of equations (4) and (5) which display the electric field components of the fibre show that the fibre field acquires not only two individual transverse (radial and azimuthal) components but also a longitudinal (axial) component. The existence of the common phase factor $\mathrm{e}^{i\ell\varphi}$ in equation (3). means that there is an azimuthal-phase dependence. Such a phase dependence is characteristic of the field in fibre modes and is directly responsible for the orbital angular momentum content of the mode.

Figure 2 displays radial variations of the field components within the core of the fibre $(\rho < a)$ and outside it $(\rho > a)$ for optical fibre mode EH for which $(\ell = 2, m = 1)$. The refractive indices of the fibre and the vacuum cladding are $n_1 = 1.4615$ and $n_2 = 1$.

2.2. Dispersion relation

For a fibre mode of frequency ω, wavelength $\lambda = 2\pi c/\omega$ and wave number $k = \omega/c$, the propagation constant β satisfies the transcendental equation [20]

$$\begin{aligned}
&\left[\frac{J'_{\ell}(\mu a)}{\mu a J_{\ell}(\mu a)} + \frac{K'_{\ell}(\nu a)}{\nu a K_{\ell}(\nu a)}\right]\left[\frac{n_1^2 J'_{\ell}(\mu a)}{\mu a J_{\ell}(\mu a)} + \frac{n_2^2 K'_{\ell}(\nu a)}{\nu a K_{\ell}(\nu a)}\right] \\
&\qquad = \left(\frac{\ell\beta}{k}\right)^2\left(\frac{1}{\mu^2 a^2} + \frac{1}{\nu^2 a^2}\right)^2.
\end{aligned} \tag{8}$$

The case $\ell = 0$ is concerned with the TE and TM modes, but we are interested here in the case $\ell \neq 0$, so equation (8). involves a mixture of HE and EH modes [20–22]. For HE modes we have

$$f_{\mathrm{HE}}(\beta) = \frac{J_{\ell-1}(\mu a)}{\mu a J_{\ell}(\mu a)} - \frac{\ell}{\mu^2 a^2} + \frac{1}{2}\left(1 + \frac{n_2^2}{n_1^2}\right)\frac{K'_{\ell}(\nu a)}{\nu a K_{\ell}(\nu a)} + \mathcal{A} = 0. \tag{9}$$

The dispersion relation for the EH modes differs by the negative sign multiplying $\mathcal{A}$ and so on evaluation it gives rise to different values of β

$$f_{\mathrm{EH}}(\beta) = \frac{J_{\ell-1}(\mu a)}{\mu a J_{\ell}(\mu a)} - \frac{l}{\mu^2 a^2} + \frac{1}{2}\left(1 + \frac{n_2^2}{n_1^2}\right)\frac{K'_{\ell}(\nu a)}{\nu a K_{\ell}(\nu a)} - \mathcal{A} = 0, \tag{10}$$

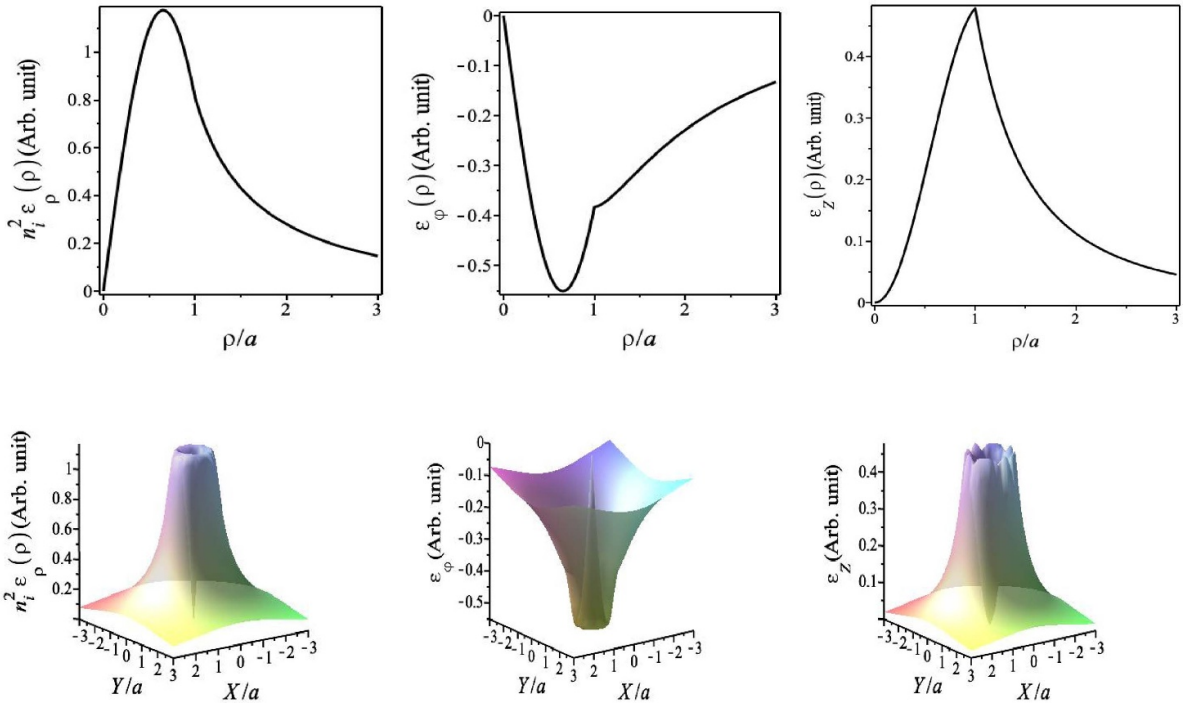

Figure 2. Upper panel: variations of the field components $\mathcal{E}_\rho, \mathcal{E}_\varphi, \mathcal{E}_z$ with the radial coordinate ρ for the EH optical fibre mode for which $(\ell = 2, m = 1)$. Lower panel: variations in the XY plane indicating cylindrical symmetry. The refractive indices of the fibre core material and the vacuum cladding are $n_1 = 1.4615$ and $n_2 = 1$, respectively. The fibre radius is $a = 290$ nm and the wavelength of the light is set to $\lambda = 685$ nm.

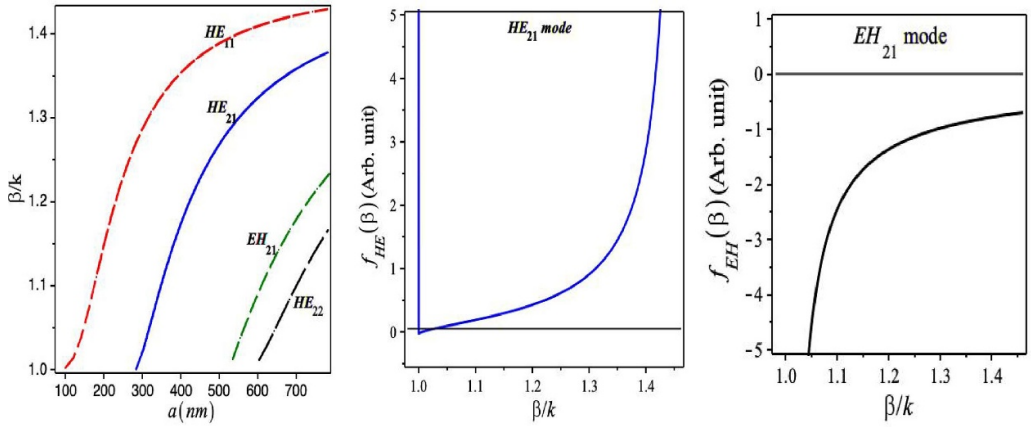

Figure 3. Left panel: variations of the scaled propagation constant β/k with the fibre radius a. The wavelength of the light is set to $\lambda = 685$ nm. Middle and right panels: variations of the dispersion functions f_{HE} and f_{EH} with β/k for $\ell = 2$ $m = 1$. The roots of the dispersion functions determine the values of β in each case. Once again, the refractive indices of the fibre and the vacuum cladding are assumed to be $n_1 = 1.4615$ and $n_2 = 1$, and the fibre radius is $a = 290$ nm.

where $\mathcal{A}$ is given by

$$\mathcal{A} = \left[\left(\frac{\ell\beta}{n_1 k}\right)^2 \left(\frac{1}{\nu^2 a^2} + \frac{1}{h^2 a^2}\right)^2 + \frac{1}{4}\left(1 - \frac{n_2^2}{n_1^2}\right)^2 \left(\frac{K'_\ell(\nu a)}{\nu a K_\ell(qa)}\right)^2\right]^{1/2}. \tag{11}$$

The HE and EH modes are labelled by $\mathrm{HE}_{\ell m}$ and $\mathrm{EH}_{\ell m}$, respectively, such that $\ell = 1, 2, \ldots$ and $m = 1, 2, \ldots$ are the azimuthal and radial mode orders, respectively. In this case, the radial mode order m indicates that the $\mathrm{HE}_{\ell m}$ or $\mathrm{EH}_{\ell m}$ mode is the solution to the corresponding equation (9) or (10).

Figure 3 (left panel) displays the variations of the propagation constant of the fibre as a function of the fibre radius a at optical wavelength $\lambda = 685$ nm for the fundamental HE_{11} mode as well as some higher-order modes. However, for the optical fibre under consideration here the higher-order mode, HE_{21} is realisable at $a \simeq 283$ nm. It is well-known that as the fibre radius a increases the number of modes it can

support increases. Our numerical results agree with those in the literature [13, 24–26].

Figure 3 (middle and right panels), display the dispersion functions (9) and (10) against β/k for the HE, EH with $(\ell = 2)$ where the fibre radius $a = 290\,\text{nm}$. The refractive indices of the fibre and the vacuum cladding are $n_1 = 1.4615$ and $n_2 = 1$, respectively.

3. Quadrupole interaction

3.1. Derivation of the Rabi frequency

Having described both the mode functions and the dispersion relations of the hybrid fibre modes with which the atomic two-level system interacts, we now turn to describe the two-level system itself as consisting of a two-level atom engaging with the fibre through its electric quadrupole moment. The ground and excited states of the two-level-atom involved in the atomic quadrupole transition are $\{|g\rangle, |e\rangle\}$ with corresponding frequencies ω_g and ω_e, respectively, corresponding to the resonance frequency $\omega_a = (\omega_e - \omega_g)$. The interaction Hamiltonian is written in Cartesian coordinate systems as a multipolar series with fields evaluated at the centre of mass coordinate $\mathbf{R} = (X, Y, Z)$ and can be written as [27–32]

$$\hat{H}_{\text{int}} = \hat{H}_D + \hat{H}_Q + \ldots, \tag{12}$$

where the first term $\hat{H}_D = -\hat{\boldsymbol{d}}.\hat{\mathbf{E}}(\mathbf{R})$ stands for the electric dipole interaction between the neutral atom and the electric field, $\hat{\boldsymbol{d}}$ is the electric dipole moment vector, where $\mathbf{r} = (x, y, z)$ is the internal electronic-type position vector with components (x, y, z) written as x_i, $i = 1, 2, 3$. $\hat{\boldsymbol{E}}(\mathbf{R})$ is the electric field vector evaluated at the centre of mass coordinate $\mathbf{R}$. The atomic transition process in question is taken here to be dipole-forbidden but quadrupole-allowed, so it is the second (quadrupole) interaction term in equation (12) that dominates in this case. We have

$$\hat{H}_Q = -\frac{1}{2}\sum_{ij} \hat{Q}_{ij} \nabla_i \hat{E}_j. \tag{13}$$

This is essentially the interaction involving the Cartesian components of the quadrupole moment tensor $\hat{Q}_{ij} = e x_i x_j$ and the gradients of the electric field vector components, evaluated at the centre-of-mass coordinate $\mathbf{R}$. Here ∇_i are components of the $\boldsymbol{\nabla}$ vector operator which act only on the spatial coordinates of the transverse electric field vector $\mathbf{E}$ as a function of the centre of mass vector $\mathbf{R} = (X, Y, Z)$.

For the two-level atom, the quadrupole tensor operators $\hat{Q}_{ij}$ can be written in terms of ladder operators as $\hat{Q}_{ij} = Q_{ij}(\hat{b} + \hat{b}^\dagger)$, where $Q_{ij} = \langle i|\hat{Q}_{ij}|j\rangle$ are the quadrupole matrix elements between the two atomic levels, and $\hat{b}(\hat{b}^\dagger)$ are the atomic level lowering (raising) operators. The electric field equation (3) can now be written in the Cartesian form

$$\mathbf{E}(\mathbf{R}) = \sum_i \hat{\mathbf{e}}_i E_i, \tag{14}$$

where $\hat{\mathbf{e}}_i (i = x, y, z)$ are the Cartesian unit vectors and E_i are the Cartesian components of the optical electric field that can be written as

$$E_i = u_i^{\{\alpha\}}(\mathbf{R})\, \mathrm{e}^{i\theta^{\{\alpha\}}(\mathbf{R})} e^{-i\omega t} + c.c., \tag{15}$$

where c.c. stands for complex conjugate; $u_i^{\alpha}(\mathbf{R})$ and $\theta^{\alpha}(\mathbf{R})$ are the amplitude and the phase functions of the Cartesian ith optical electric field component. Recall that the superscript α denotes a group of indices that specify the optical mode in terms of its frequency ω, the mode kind C, azimuthal and radial numbers ℓ and m, and the polarisation index p. The quadrupole interaction Hamiltonian can now be written as follows

$$\hat{H}_Q = -\frac{1}{2}\sum_{i,j} \hat{Q}_{ij} \frac{\partial E_j}{\partial R_i}. \tag{16}$$

and this interaction Hamiltonian can also be written in terms of the Rabi frequency as follows

$$\hat{H}_Q = -\hbar \Omega_Q^{\{\alpha\}}(\mathbf{R})\, \hat{a} e^{i\theta^{\{\alpha\}}(\mathbf{R})} e^{-i\omega t} + H.c. \tag{17}$$

where $\hat{a}$ and $\hat{a}^\dagger$ are the fibre mode destruction and creation operators and $\Omega_Q^{\{\alpha\}}(\mathbf{R})$ is the quadrupole Rabi frequency

$$\Omega_Q^{\{\alpha\}}(\mathbf{R}) = \frac{1}{2\hbar}\sum_{i,j} Q_{ij} u_j^{\{\alpha\}} \left(\frac{1}{u_j^{\{\alpha\}}} \frac{\partial u_j^{\{\alpha\}}}{\partial R_i} + i \frac{\partial \theta^{\{\alpha\}}}{\partial R_i} \right) \tag{18}$$

This is the general form of the quadrupole Rabi frequency which applies to any of the allowed modes.

Recall that the optical fibre is a long dielectric cylinder of radius a and refractive index n_1 immersed in a background medium of refractive index n_2, where $n_2 < n_1$. The Quadrupole interaction is expressed in terms of the Cartesian coordinates $\{x, y, z\}$ relative to the atomic centre of mass, with the centre of mass coordinate written $\mathbf{R} = (X, Y, Z)$. The amplitude functions of the electric field components of the fibre modes $\mathcal{E}_j$ are, however, given in cylindrical coordinates $\mathbf{R} = (\rho, \varphi, Z)$, so to proceed we need to make a transformation to express the optical electric field components of the fibre modes in terms of $u_j^{\{\alpha\}}(\mathbf{R})$. We have

$$\begin{aligned} u_x^{\{\alpha\}} &= \cos(\varphi)\,\mathcal{E}_\rho - \sin(\varphi)\,\mathcal{E}_\varphi, \\ u_y^{\{\alpha\}} &= \sin(\varphi)\,\mathcal{E}_\rho + \cos(\varphi)\,\mathcal{E}_\varphi, \\ u_z^{\{\alpha\}} &= \mathcal{E}_Z, \end{aligned} \tag{19}$$

where $\theta^{\{\alpha\}} = (s\beta Z + p\ell\varphi)$. Also $\rho = \sqrt{X^2 + Y^2}$ and $\varphi = \tan^{-1}(Y/X)$. The quadrupole Rabi frequency equation (18) can now be written as the sum of three terms

$$\Omega_Q^{\{\alpha\}}(\mathbf{R}) = \frac{1}{2\hbar}\sum_{j=1}^{3} \Omega_j, \tag{20}$$

where

$$\Omega_1 = \left(\frac{\partial u_x^{\{\alpha\}}}{\partial X} - i\xi_1 u_x^{\{\alpha\}}\right) Q_{xx} + \left(\frac{\partial u_y^{\{\alpha\}}}{\partial X} - i\xi_1 u_y^{\{\alpha\}}\right) Q_{xy} + \left(\frac{\partial u_z^{\{\alpha\}}}{\partial X} - i\xi_1 u_z^{\{\alpha\}}\right) Q_{xz},$$
$$\Omega_2 = \left(\frac{\partial u_x^{\{\alpha\}}}{\partial Y} + i\xi_2 u_x^{\{\alpha\}}\right) Q_{yx} + \left(\frac{\partial u_y^{\{\alpha\}}}{\partial Y} + i\xi_2 u_y^{\{\alpha\}}\right) Q_{yy} + \left(\frac{\partial u_z^{\{\alpha\}}}{\partial Y} + i\xi_2 u_z^{\{\alpha\}}\right) Q_{yz},$$
$$\Omega_3 = is\beta\left(u_x^{\{\alpha\}} Q_{zx} + u_y^{\{\alpha\}} Q_{zy} + u_z^{\{\alpha\}} Q_{zz}\right), \tag{21}$$

where $\xi_1 = p\ell Y/(X^2+Y^2)$ and $\xi_2 = p\ell X/(X^2+Y^2)$. For an absorption transition, the quadrupole Rabi frequency depends on the type of mode excited in the optical fibre involved in the quadrupole transition and the angular momentum quantum numbers of the two energy levels, and these are governed by the transition selection rules.

3.2. Applying the selection rules

We focus specifically on the quadrupole transition $|L=0, m_l=0\rangle \to |L=2, m_l'\rangle$ in which a fibre mode is absorbed, where $(m_l' = 0, \pm 1, \pm 2)$ and we are adopting the notation $|L, m_l\rangle$ for the atomic state, labeled by the angular momentum quantum numbers [27–30].

The selection rules are $\Delta L = 0, \pm 2$; $\Delta m = 0, \pm 1, \pm 2$. We consider the following three situations

- For the case $m_l' = 0$, the quadrupole moment tensor can be evaluated [27, 28] and we find that all the off-diagonal quadrupole tensor components are equal to zero $(Q_{xy} = Q_{xz} = Q_{yz} = 0)$, while the diagonal matrix elements are non-zero. We have $(Q_{xx} = Q_{yy} = Q_0$ and $Q_{zz} = -2Q_0)$. Thus, the Rabi frequency equation (20) takes the following simpler form,

$$\Omega_Q^{\{\alpha\}}(\mathbf{R}) = \frac{Q_0}{2\hbar}\left[\left(\frac{\partial u_x^{\{\alpha\}}}{\partial X} - i\xi_1 u_x^{\{\alpha\}}\right) + \left(\frac{\partial u_y^{\{\alpha\}}}{\partial Y} + i\xi_2 u_y^{\{\alpha\}}\right) - 2is\beta u_z^{\{\alpha\}}\right]. \tag{22}$$

Equation (22) can be written entirely in terms of the components of $\boldsymbol{\mathcal{E}}$ with cylindrical coordinates. We find

$$\Omega_Q^{\{\alpha\}}(\mathbf{R}) = \frac{Q_0}{\hbar}\left[\frac{1}{\rho}\frac{\partial(\rho\mathcal{E}_\rho)}{\partial\rho} + \frac{ip\ell}{\rho}\mathcal{E}_\varphi - 2is\beta\mathcal{E}_Z\right]. \tag{23}$$

- For the case $m_l' = \pm 1$, the diagonal matrix elements are zero $(Q_{xx} = Q_{yy} = Q_{zz} = 0)$ and the off-diagonal matrix elements are $Q_{xy} = 0$ and $Q_{xz} = iQ_1, Q_{yz} = \mp Q_1$. Consequently, the Rabi frequency equation (20) yields,

$$\Omega_Q^{\{\alpha\}}(\mathbf{R}) = \frac{Q_1}{2\hbar}\left[i\left(\frac{\partial u_z^{\{\alpha\}}}{\partial X} - i\xi_1 u_z^{\{\alpha\}}\right) \mp \left(\frac{\partial u_z^{\{\alpha\}}}{\partial Y} + i\xi_2 u_z^{\{\alpha\}}\right) + is\beta\left(iu_x^{\{\alpha\}} \mp u_y^{\{\alpha\}}\right)\right], \tag{24}$$

or in terms of the cylindrical components, we have for the case $m_l' = \pm 1$

$$\Omega_Q^{\{\alpha\}}(\mathbf{R}) = \frac{iQ_1 e^{\pm i\varphi}}{\hbar}\left[\frac{\partial\mathcal{E}_Z}{\partial\rho} \mp \frac{ip\ell}{\rho}\mathcal{E}_Z + is\beta(\mathcal{E}_\rho \pm i\mathcal{E}_\varphi)\right]. \tag{25}$$

- For the case $m_l' = \pm 2$, the zero matrix elements are $(Q_{zz} = Q_{yz} = Q_{xz} = 0)$ and the non zero matrix elements are $Q_{xx} = -Q_{yy} = Q_1, Q_{xy} = \pm iQ_1$. Accordingly, the Rabi frequency equation (20) has the following form,

$$\Omega_Q^{\{\alpha\}}(\mathbf{R}) = \frac{Q_1}{\hbar}\left[\left(\frac{\partial u_x^{\{\alpha\}}}{\partial X} - i\xi_1 u_x^{\{\alpha\}}\right) - \left(\frac{\partial u_y^{\{\alpha\}}}{\partial Y} + i\xi_2 u_y^{\{\alpha\}}\right) \pm i\left(\left(\frac{\partial u_y^{\{\alpha\}}}{\partial X} - i\xi_1 u_y^{\{\alpha\}}\right) + \left(\frac{\partial u_x^{\{\alpha\}}}{\partial Y} + i\xi_2 u_x^{\{\alpha\}}\right)\right)\right], \tag{26}$$

and in terms of the cylindrical components, we have for the case $m_l' = \pm 2$

$$\Omega_Q^{\{\alpha\}}(\mathbf{R}) = \frac{Q_1 e^{\pm 2i\varphi}}{\hbar}\left[\left(\frac{\partial}{\partial\rho}(\mathcal{E}_\rho \pm i\mathcal{E}_\varphi) - \frac{1}{\rho}(1 \pm p\ell)(\mathcal{E}_\rho \pm i\mathcal{E}_\varphi)\right)\right]. \tag{27}$$

We thus have in hand closed expressions for the Rabi frequencies in the hybrid modes of the optical fibre for the quadrupole transitions $|L=0, m_l=0\rangle \to |L=2, m_l'\rangle$ which satisfy the transition selection rules.

4. Caesium atoms outside optical fibre

Once again we emphasise that we are investigating the specific case of the Cs atom, which has also been the subject of an investigation involving its quadrupole transition $(6^2S_{1/2} \to 5^2D_{5/2})$ in various contexts [12, 17, 30, 33, 34]. We have the following as parameters for Cs: $\lambda = 685$ nm, $Q_{xx} = 10ea_0^2$ (with a_0 the Bohr radius), and the de-excitation rate involved in the quadrupole transition $\gamma = 7.8 \times 10^5\,(\mathrm{s}^{-1})$. The fibre radius is $a = 290$ nm and the refractive indices of the fibre core and the vacuum cladding are $n_1 = 1.4615$ and $n_2 = 1$, respectively. The overall constant $\mathcal{N}$ depends on the power $\mathcal{P}$ of the excited fibre mode and here we set the value of $\mathcal{P}$ as $\mathcal{P} = 2.5\,(\mu\mathrm{W})$ [15].

In appendix B we evaluate the components of the Poynting vector and exhibit their variations with the atom position $\rho \geqslant a$ outside fibre. It is clear that the azimuthal component is

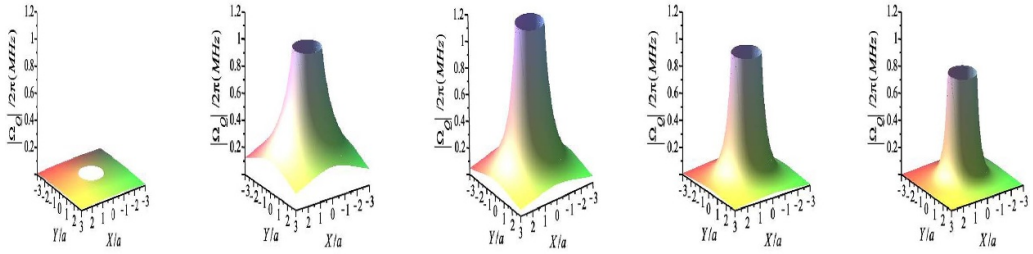

Figure 4. The spatial distribution of the quadrupole Rabi frequency $|\Omega_Q|/2\pi\,(\mathrm{kHz})$ for the Cs atom with the quadrupole transition $|L=0,m_l=0\rangle \rightarrow |L=2,m_l'\rangle$ in the mode $C=\{\mathrm{HE}_{21}\}$. For $m_l'=-2$, $m_l'=-1$, $m_l'=0$, $m_l'=+1$, and $m_l'=+2$ from the left to the right, respectively. In all cases $s=+1, p=+1$. The power is $\mathcal{P}=2.5$ (μW); for other parameters see the text.

much smaller than the axial component and we conclude that equation (1) is reasonably well satisfied. We may now consider the processes of absorption of the hybrid optical fibre modes by the atom, having obtained expressions for their Rabi frequencies in preparation for evaluating the absorption rate.

4.1. Absorption of an HE mode

An HE mode is appropriate for the quadrupole transition $|L=0,m_l=0\rangle \rightarrow |L=2,m_l'\rangle$ for the mode $C=\{\mathrm{HE}_{\ell m}\}$. We need not substitute $\ell=2$ at this stage, then using equation (5) and assuming $p=1$, we need to evaluate the quadrupole Rabi frequencies for the different situations.

For the case $m_l'=0$, equation (23) becomes

$$\Omega_Q^{\{\alpha\}}(\mathbf{R}) = -i\frac{Q_0}{2\hbar}\beta(2s+1)\mathcal{N}\frac{J_\ell(\mu a)}{K_\ell(\nu a)}K_\ell(\nu\rho) \tag{28}$$

For the case $m_l'=\pm1$, equation (25) reads

$$\Omega_Q^{\{\alpha\}}(\mathbf{R}) = \pm i\frac{Q_1}{2\hbar}\mathcal{N}\mathrm{e}^{\pm i\varphi}\frac{J_\ell(\mu a)}{K_\ell(\nu a)}\left((i\pm1)\frac{\ell}{\rho}K_\ell(\nu\rho) + \frac{s\beta^2(\xi\pm1)\pm\nu^2}{\nu}K_{\ell+1}(\nu\rho)\right). \tag{29}$$

and we note the explicit appearance of the index $s=\pm1$, the direction of polarisation in the above expressions.

For the case $m_l'=\pm2$ we obtain from equation (27)

$$\Omega_Q^{\{\alpha\}}(\mathbf{R}) = \mp i\frac{Q_1}{2\hbar}\beta(\xi\pm1)\mathcal{N}\mathrm{e}^{\pm i2\varphi}\frac{J_\ell(\mu a)}{K_\ell(\nu a)} \times\left(K_\ell(\nu\rho)+\frac{2(1\pm\ell)}{\nu\rho}K_{\ell\pm1}(\nu\rho)\right), \tag{30}$$

which does not depend on $s=\pm1$.

We have to include the Clebsch–Gordan coefficients (CGC) in the formalism since the atomic levels involve both the orbital angular momentum and the spin of the electron, both of which are required in fine structure. The following CGCs

$$\mathrm{CGC}=\sqrt{\frac{5}{5}},\quad\sqrt{\frac{4}{5}},\quad\sqrt{\frac{3}{5}},\quad\sqrt{\frac{2}{5}},\quad\sqrt{\frac{1}{5}}, \tag{31}$$

correspond to the transitions for which $\Delta m=-2,-1,0,+1,+2$, respectively [32, 35].

Figure 4 displays the spatial distribution of the quadrupole Rabi frequency $|\Omega_Q/2\pi\,(\mathrm{kHz})|$ for the Cs atom with the quadrupole transition $|L=0,m_l=0\rangle \rightarrow |L=2,m_l'\rangle$ in the mode $C=\{\mathrm{HE}_{21}\}$ where $\ell=2$ for different values of $m_l'=0,\pm1,\pm2$. The results show that the quadrupole Rabi frequency has cylindrical symmetry and exhibits the usual characteristic dependence of decaying amplitude with the radial distance outside the fibre ($\rho>a$). It is clear from these results that the largest magnitude of the quadrupole Rabi frequency corresponds to the case of the quadrupole transition $|L=0,m_l=0\rangle \rightarrow |L=2,m_l'=0\rangle$.

In order to explore the effect of the direction of the propagation of light in the nano-fibre on the quadrupole Rabi frequency, we present in figures 5(a)–(c), the radial variation of the quadrupole Rabi frequency $|\Omega_Q|/2\pi\,(\mathrm{kHz})$ for the Cs atom with the quadrupole transition $|L=0,m_l=0\rangle \rightarrow |L=2,m_l'\rangle$ in the mode $C=\{\mathrm{HE}_{21}\}$ for $m_l'=0,\pm1.\pm2$ and different directions of propagation $s=\pm1$. So the quadrupole transition $|L=0,m_l=0\rangle \rightarrow |L=2,m_l'=\pm2\rangle$ does not depend on the direction of the propagation, as has been shown previously.

Whenever the index s has the value $s=-1$ we find that the magnitude of the quadrupole Rabi frequency is smaller than that for the corresponding case where $s=+1$ for the cases ($m_l'=0,\pm1$).

It is also of interest to examine the effect of the polarisation index p of light in the nano fibre on the quadrupole Rabi frequency, so figure 6 shows the radial variations of the absolute value of the quadrupole Rabi frequency $|\Omega_Q|/2\pi\,(\mathrm{kHz})$ for the Cs atom quadrupole transition $|L=0,m_l=0\rangle \rightarrow |L=2,m_l'\rangle$ in the mode $C=\{\mathrm{HE}_{21}\}$ for $m_l'=0,\pm1,\pm2$ and different value of the polarisation parameter $p=\pm1$. It is seen that the magnitude of the quadrupole Rabi frequency is affected by the polarisation index p and the maximum magnitude corresponds to the last panel for $m_l'=-2$, $s=\pm1$, and $p=-1$.

The fact that we obtain different values for the Rabi frequency for different directions of propagation is a chirality effect, as described by the interesting work of Rauschenbeutel *et al* [13, 36–38].

The Rabi frequency in general shows a decrease with the radial position in all the curves shown here plotted with different parameters, except for the red dashed curve in figure 6(b). This shows a slight increase close to the fibre, leading to a shallow maximum, followed by a general

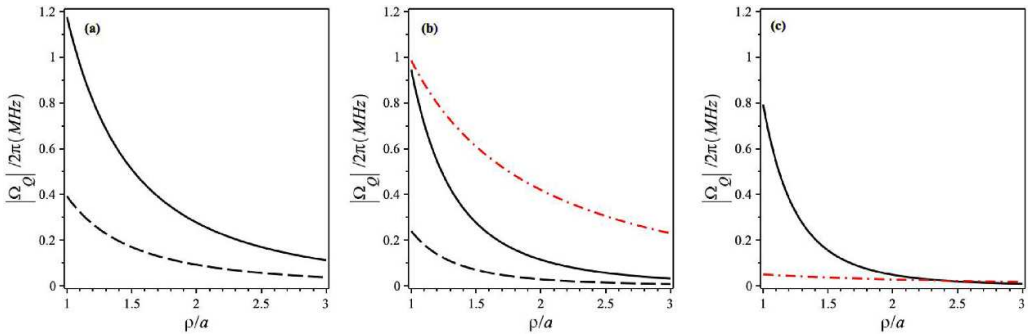

Figure 5. Variations of the quadrupole Rabi frequency $|\Omega_Q|/2\pi$ (kHz) with ρ for the quadrupole transition $|L=0,m_l=0\rangle \rightarrow |L=2,m_l'\rangle$ in Cs. The plots are for different values of the propagation index $s=\pm 1$. (a)–(c) For the mode $C=\{\mathrm{HE}_{21}\}$. (a) For $m_l'=0$. (b) For $m_l'=+1$ (black solid line) and for $m_l'=-1$ (red dash-dotted line). (c) For $m_l'=+2$ (black solid line) and $m_l'=-2$ (red dash-dotted line) . The dashed line in all panels concerns the case $s=-1$, while the solid line is for $s=+1$. In all cases $p=+1$. The power is $\mathcal{P}=2.5$ (μW); for other parameters see the text.

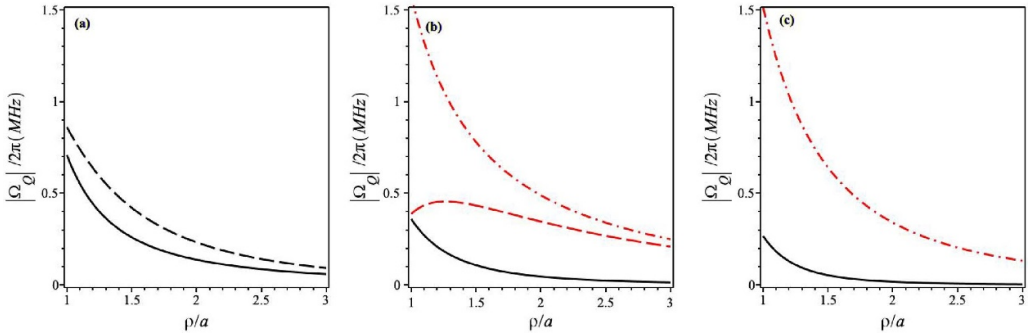

Figure 6. Variations of the quadrupole Rabi frequency $|\Omega_Q|/2\pi$ (kHz) with ρ for the Cs atom quadrupole transition $|L=0,m_l=0\rangle \rightarrow |L=2,m_l'\rangle$. The plots are for different values of the propagation $s=\pm 1$. (a)–(c) For the mode $C=\{\mathrm{HE}_{21}\}$. (a) For $m_l'=0$. (b) for $m_l'=+1$ (black solid line) and for $m_l'=-1$ (red dashed line). (c) For $m_l'=+2$ (black solid line) and $m_l'=-2$ (red dash-dotted line) . The dashed line in all panels is for the case $s=-1$, while the solid and dash-dotted lines are for $s=+1$. In all cases $p=-1$. The power is $\mathcal{P}=2.5$ (μW); for other parameters see the text.

decrease as for other curves. This behaviour can be explained with reference to equation (25). It is seen that in the case where both s and p are negative, the general tendency to decrease controlled by the p term is initially dominated by the s-dependent term which then diminishes with the radial position.

Having evaluated the quadrupole Rabi frequency for the different cases allowed by the selection rules and by the optical fibre parameters our final task is to evaluate the corresponding quadrupole transition rates.

5. Transition amplitude and absorption rate

The transition matrix element [8, 27], comprising only the quadrupole interaction, is $\mathrm{M}_{if}^{\{\alpha\}}=\langle f|\hat{H}_Q|i\rangle$, where $|i\rangle$ and $|f\rangle$ are, respectively, the initial and final states of the overall quantum system (atom plus fibre mode). We assume that the system has as an initial state $|i\rangle$ with the atom in its ground state and there is one optical fibre photon. The final state $|f\rangle$ consists of the excited state of the atom and there is no field mode. Thus $|i\rangle=|g\{1\}_{\{\alpha\}}\rangle$ and $|f\rangle=|e\{0\}\rangle$. We make use of the relations $\langle\{0\}|\hat{a}^{+}_{\{\alpha'\}}|\{1\}_{\{\alpha\}}\rangle=0$ and $\langle\{0\}|\hat{a}_{\{\alpha'\}}|\{1\}_{\{\alpha\}}\rangle=\delta_{\{\alpha'\}\{\alpha\}}$, where $a_{\{\alpha\}}$ and $a^{\dagger}_{\{\alpha\}}$ are the annihilation and creation operators of the fibre mode α. We obtain

$$\mathrm{M}_{if}^{\{\alpha\}}=\hbar\Omega_Q^{\{\alpha\}}(\mathbf{R})\,\mathrm{e}^{i\theta^{\{\alpha\}}(\mathbf{R})} \tag{32}$$

where $\Omega_Q^{\{\alpha\}}(\mathbf{R})$ is the quadrupole Rabi frequency. The final state of the system in the absorption process comprises a continuous band of energy of width $\hbar\gamma$ where γ is the de-excitation rate involved in the quadrupole transition. In this case, the absorption rate is governed by the form of Fermi's golden rule [27, 39] with a density of states

$$\Gamma_{if}=2\pi\left|\Omega_Q^{\{\alpha\}}(\mathbf{R})\right|^2\rho_{\omega_a}(\omega)\,, \tag{33}$$

where $\rho_{\omega_a}(\omega)$ is the density of the final state which is well represented by a Lorentzian distribution of states of width (FWHM) matching the free space spontaneous quadrupole emission rate. Thus

$$\rho_{\omega_a}(\omega)=\frac{1}{\pi}\frac{\gamma/2}{(\omega-\omega_a)^2+(\gamma/2)^2}. \tag{34}$$

The Lorentzian distribution characterising the density of states specifies a limit to the validity of using Fermi's Golden rule to calculate the absorption rate since such a rate is valid only

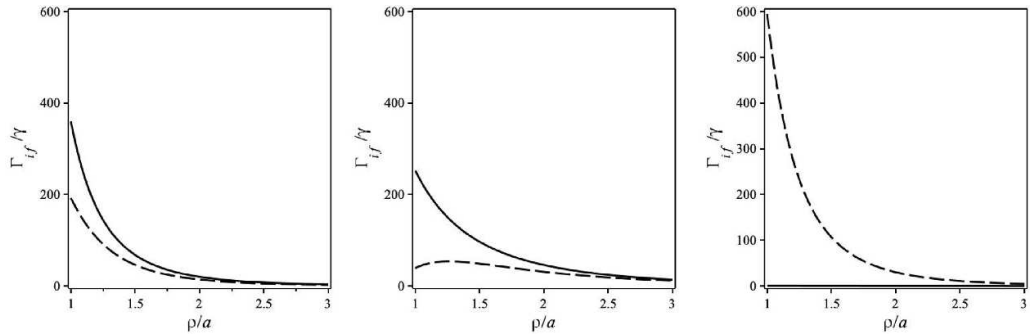

Figure 7. Variations of the quadrupole absorption rate Γ_{if}/γ for the Cs atom quadrupole transition $|L=0,m_l=0\rangle \rightarrow |L=2,m_l'\rangle$ with (a) $m_l'=0$, (b) $m_l'=-1$, and (c) $m_l'=-2$ for the mode $C=\{\mathrm{HE}_{21}\}$. Solid lines $(s=+1,p=+1)$, dashed lines $(s=-1,p=-1)$. The power is $\mathcal{P}=2.5$ (μW); for other parameters see the text. All panels indicate a huge (more than two orders of magnitude) increase in the absorption rate for atomic radial position $\rho=a$. This is attributable to the enhanced density of states just outside the fibre surface.

if the frequency width of the upper state $|e\rangle$ is larger than the excitation rate; i.e. the spontaneous emission rate is larger than the Rabi frequency. The Rabi frequency may exceed the spontaneous emission rate for high intensities, in which case the perturbative approach culminating in the Fermi Golden Rule is no longer valid and the strong coupling regime is applicable involving Rabi oscillations. Substituting equation (34) in equation (33) we find for the quadrupole absorption rate

$$\Gamma_{if}=\frac{\gamma}{(\omega-\omega_a)^2+(\gamma/2)^2}\left|\Omega_Q^{\{\alpha\}}(\mathbf{R})\right|^2. \tag{35}$$

This general expression applies to the various cases involving the different fibre modes participating in transitions satisfying the selection rules as discussed above. For illustration only, we display in figure 7, the variations of the absorption rate Γ_{if}/γ with the radial position of the atom ρ/a outside the fibre $\rho>a$. We have concentrated on the quadrupole transition $|L=0,m_l=0\rangle \rightarrow |L=2,m_l'\rangle$ for different directions of propagation $s=\pm1$ and the mode $C=\{\mathrm{HE}_{21}\}$. It can be seen for this particular case the absorption rate decreases with increasing ρ and it is independent of the phase circulation direction $p=\pm1$. Its magnitude close to the fibre surface $\rho\approx a$ can be more than two orders of magnitude relative to γ. The corresponding orbital angular momentum transfer rate in the case of $\Delta L=2$ is simply $2\hbar\Gamma_{if}$.

6. Conclusions

In conclusion, we have systematised the formalism leading to the evaluation of the quadrupole absorption rate in the case of two-level systems localised outside the surface of an optical nano-fibre with a step-index profile, leading to modes that decay with radial distance outside the fibre. The evaluation of the rates required, as a first step, the determination of the quadrupole Rabi frequencies for the hybrid modes in the optical fibre. The quadrupole selection rules determine the form of the different types of field distribution that enters the coupling of the fields to the quadrupole moments. Once the quadrupole Rabi frequencies are determined the absorption rate follows using the Fermi Golden rule with a Lorentzian final density of states function for the upper atomic level.

The hybrid modes are characterised by several special features which impact the evaluation of the absorption rates. Firstly these modes influence the form of the quadrupole tensor components that enter a specific interaction with the electric field gradients. Also, the absorption process involves a transaction between the fibre modes and the two-level system in which a quantum with specific characteristics is absorbed. Other characteristics of the fibre modes that affect the interaction are whether the mode is propagating along the $+z$ direction, or $-z$ direction and whether the helical rotation is clockwise or anti-clockwise. Such aspects will need to be taken into account in the context of actual experimental measurements. The observation that the results depend on the direction of propagation is interesting as has been pointed out recently by Ladahl *et al* [38, 40]) who, appropriately, referred to such a feature as a chirality effect.

We have focused on the quadrupole transition in Cs primarily because this quadrupole transition has been the subject of recent investigations involving the interaction of Cs in the fields of optical fibres. We have chosen to consider the simplest type of optical fibre with a uniform core material of refractive index $n_1>1$ immersed in free space. Various other forms of optical fibre can be considered in which the core material is enclosed in a thin metallic layer, or a doped semiconductor in which case the dielectric function may be frequency- and wave vector-dependent and may have a complicated profile. The uniform core fibre system discussed here has led to results for the absorption rate, as shown in figure 7, which should be experimentally measurable. Note that we have expressed the absorption rate Γ_{if} in terms of γ whose value is known for Cs and we have considered it a good scaling parameter to use in this context as done in a recent experiment [15]. Note also that we have considered only one specific value of the input power $\mathcal{P}$ used to excite the fibre mode with which the atom interacts. Similar evaluations can be carried out for other value of $\mathcal{P}$. From figure 7 we can see that the absorption rate can be at least two orders of magnitude larger than γ and are amenable to experimental measurements.

Data availability statement

All data that support the findings of this study are included within the article (and any supplementary files).

Acknowledgments

The authors are grateful to Professors Stephen Barnett, Sile Nic Chormaic, and Fam Le Kien for useful correspondence.

Appendix A. Evaluation of $\mathcal{N}$

The overall constant field amplitude $\mathcal{N}$ is fixed in terms of the experimentally controlled applied cycle-averaged field power $\mathcal{P}$ which is formally defined as the surface integral of the Poynting vector over a cross-section of the fibre. To evaluate this in the case of the fibre modes we need expressions for the magnetic field components of the fibre nodes which are as follows

Hybrid modes:

- In the core region $0 \leqslant \rho \leqslant a$ we have:

$$\begin{aligned}
\mathcal{H}_\rho &= i\mathcal{N}\frac{\omega\varepsilon_0 n_1^2}{2\mu}\left[(1-\sigma_1)J_{\ell-1}(\mu\rho)+(1+\sigma_1)J_{\ell+1}(\mu\rho\right],\\
\mathcal{H}_\varphi &= \mathcal{N}\frac{\omega\varepsilon_0 n_1^2}{2\mu}\left[(1-\sigma_1)J_{\ell-1}(\mu\rho)-(1+\sigma_1)J_{\ell+1}(\mu\rho)\right],\\
\mathcal{H}_Z &= -\mathcal{N}\frac{\beta}{\omega\mu_0}\xi J_\ell(\mu\rho),
\end{aligned} \tag{A.1}$$

- In the cladding (vacuum) region $\rho > a$ we have

$$\begin{aligned}
\mathcal{H}_\rho &= i\mathcal{N}\frac{\omega\varepsilon_0 n_2^2}{2\nu}\frac{J_\ell(\mu a)}{K_\ell(\nu a)}\\
&\quad\times\left[(1-\sigma_2)K_{\ell-1}(\nu\rho)-(1+\sigma_2)K_{\ell+1}(\nu\rho)\right],\\
\mathcal{H}_\varphi &= i\mathcal{N}\frac{\omega\varepsilon_0 n_2^2}{2\nu}\frac{J_\ell(\mu a)}{K_\ell(\nu a)}\\
&\quad\times\left[(1-\sigma_2)K_{\ell-1}(\nu\rho)-(1+\sigma_2)K_{\ell+1}(\nu\rho)\right],\\
\mathcal{H}_Z &= -\mathcal{N}\frac{\beta}{\omega\mu_0}\xi\frac{J_\ell(\mu a)}{K_\ell(\nu a)}K_\ell(\nu\rho),
\end{aligned} \tag{A.2}$$

where

$$\sigma_1 = \frac{\beta^2}{k^2 n_1^2}\xi, \quad \sigma_2 = \frac{\beta^2}{k^2 n_2^2}\xi. \tag{A.3}$$

The time-averaged Poynting vector component along the z-axis per unit area is expressed as

$$S_Z = \frac{1}{2}(\mathbf{E}\times\mathbf{H}^*)\cdot\hat{u}_Z = \frac{1}{2}\left(\mathcal{E}_\rho\mathcal{H}_\varphi^* - \mathcal{E}_\varphi\mathcal{H}_\rho^*\right), \tag{A.4}$$

where $\hat{u}_Z$ is a unit vector in the Z-direction. The power residing in a mode of the optical fibre is then given by

$$\begin{aligned}
\mathcal{P} &= \int_0^{2\pi}\int_0^\infty S_Z\,\rho\,\mathrm{d}\rho\,\mathrm{d}\varphi\\
&= \frac{1}{2}\int_0^{2\pi}\int_0^\infty\left(\mathcal{E}_\rho\mathcal{H}_\varphi^* - \mathcal{E}_\varphi\mathcal{H}_\rho^*\right)\rho\,\mathrm{d}\rho\,\mathrm{d}\varphi.
\end{aligned} \tag{A.5}$$

The analytical expressions of the power flow for the hybrid modes are quite intricate. Here we give only the equations of the power as the sum of contributions from the core and cladding regions, respectively,

$$\begin{aligned}
\mathcal{P}_{\text{core}} &= \frac{\pi}{4}\omega\varepsilon_0 n_1^2\beta|\mathcal{N}|^2\frac{a^2}{\mu^2}\left[(1-\xi)(1-\sigma_1)\int_0^a J_{\ell-1}^2(\mu\rho)\,\rho\,\mathrm{d}\rho\right.\\
&\quad\left.+(1+\xi)(1+\sigma_1)\int_0^a J_{\ell+1}^2(\mu\rho)\,\rho\,\mathrm{d}\rho\right]\\
&= |\mathcal{N}|^2\mathcal{I}_{H1}
\end{aligned} \tag{A.6}$$

$$\begin{aligned}
\mathcal{P}_{\text{clad}} &= \frac{\pi}{4}\omega\varepsilon_0 n_2^2\beta|\mathcal{N}|^2\frac{a^2 J_\ell^2(\mu a)}{\nu^2 K_\ell^2(\nu a)}\left[(1-\xi)(1-\sigma_2)\right.\\
&\quad\times\int_a^\infty K_{\ell-1}^2(\nu\rho)\,\rho\,\mathrm{d}\rho + (1+\xi)(1+\sigma_2)\\
&\quad\left.\times\int_a^\infty K_{\ell+1}^2(\nu\rho)\,\rho\,\mathrm{d}\rho\right] = |\mathcal{N}|^2\mathcal{I}_{H2}
\end{aligned} \tag{A.7}$$

where σ_1 and σ_2 are given in terms of ξ by equation (A.3) and $\mathcal{I}_{H1,H2}$ are the rest of the expressions in $\mathcal{P}_{\text{core,clad}}$.

The total power is the sum

$$\mathcal{P} = \mathcal{P}_{\text{core}} + \mathcal{P}_{\text{clad}} = |\mathcal{N}|^2\left(\mathcal{I}_{H1}+\mathcal{I}_{H2}\right). \tag{A.8}$$

Thus we have

$$|\mathcal{N}|^2 = \frac{\mathcal{P}}{\mathcal{I}_{H1}+\mathcal{I}_{H2}}. \tag{A.9}$$

The undetermined constant $\mathcal{N}$ can be determined when the total power flow $\mathcal{P}$ in optical fibre is specified.

Appendix B. Radial variations of S_φ for $\rho \geqslant a$

The time-averaged Poynting vector is

$$\mathbf{S} = \frac{1}{2}\Re(\mathbf{E}\times\mathbf{H}^*) \tag{B.1}$$

so its components in cylindrical coordinates are given as

$$\begin{aligned}
S_Z &= \frac{1}{2}\left(\mathcal{E}_\rho\mathcal{H}_\varphi^* - \mathcal{E}_\varphi\mathcal{H}_\rho^*\right),\\
S_\varphi &= \frac{1}{2}\left(\mathcal{E}_Z\mathcal{H}_\rho^* - \mathcal{E}_\rho\mathcal{H}_Z^*\right),\\
S_\rho &= \frac{1}{2}\left(\mathcal{E}_\varphi\mathcal{H}_Z^* - \mathcal{E}_Z\mathcal{H}_\varphi{}^*\right),
\end{aligned} \tag{B.2}$$

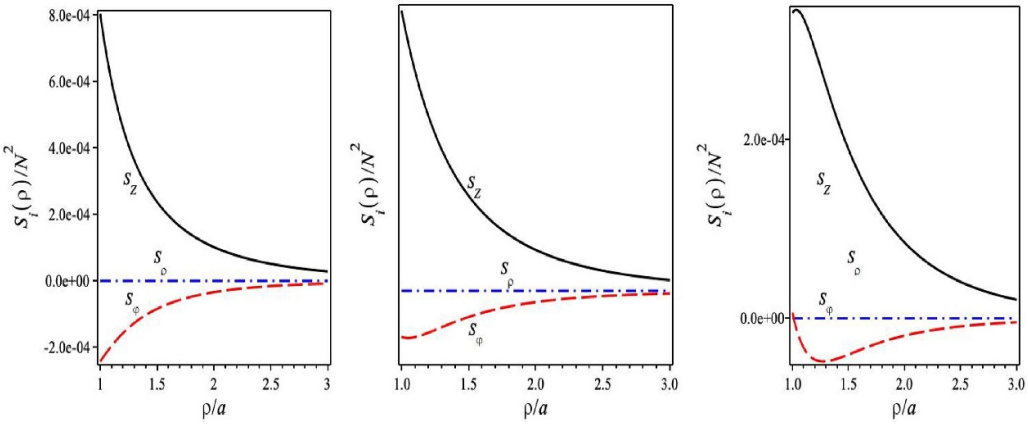

Figure B1. The radial variation of the real parts of the Poynting components for the mode $C = \{\mathrm{HE}_{21}\}$. The black solid line for S_Z. The red long-dashed line for S_φ. The blue dash-dotted line for S_ρ. Left panel: $a = 290$ nm, mid panel: $a = 340$ nm and right panel: $a = 400$ nm. For Cs $\lambda = 685$ nm. For other parameters see the text.

where the factor $1/2$ that appears in the above expressions accounts for the time average of the Poynting vector. The electric and magnetic field components are given earlier, so the evaluations are straightforward, albeit somewhat cumbersome. We, therefore, present the variations of the real parts of the Poynting vector components with radial variable ρ specifically for the mode $C = \{\mathrm{HE}_{21}\}$. The results are shown in figure B1.

It is clear that the radial component is practically zero and the azimuthal component is small compared to the z-component of the Poynting vector; i.e. $S_Z > 4S_\varphi$ for different values of the fibre radius $a = 290, 340, 400$ nm. We may now conclude that the second term in equation (2) is small, so we may assume $\mathcal{L}_z^{\mathrm{atom}} = \mathcal{L}_z^{\mathrm{fibre}}$.

ORCID iDs

S Bougouffa https://orcid.org/0000-0003-1884-4861
M Babiker https://orcid.org/0000-0003-0659-5247

References

[1] Jacob Z, Smolyaninov I I and Narimanov E E 2012 *Appl. Phys. Lett.* **100** 181105
[2] Romeira B and Fiore A 2018 *IEEE J. Quantum Electron.* **54** 2802464
[3] Gu Q and Fainman Y 2017 *Purcell Effect and the Evaluation of Purcell and Spontaneous Emission Factors* (Cambridge University Press) pp 65–90
[4] Yang Z, Bodnarchuk M I and Waks E 2017 Purcell enhanced spontaneous emission of colloidal perovskite nanocrystals *CLEO: QELS_Fundamental Science* (Optical Society of America) p FF2G.6
[5] Ruf M, Weaver M J, van Dam S B and Hanson R 2021 *Phys. Rev. Appl.* **15** 024049
[6] Rybin M V, Mingaleev S F, Limonov M F and Kivshar Y S 2016 *Sci. Rep.* **6** 20599
[7] Pan Y and Gover A 2021 *New J. Phys.* **23** 063070
[8] Scholz-Marggraf H M, Fritzsche S, Serbo V G, Afanasev A and Surzhykov A 2014 *Phys. Rev.* A **90** 013425
[9] Afanasev A, Carlson C E and Solyanik M 2017 *J. Opt.* **19** 105401
[10] Afanasev A, Carlson C E and Mukherjee A 2016 *J. Opt.* **18** 074013
[11] Chan E A, Aljunid S A, Zheludev N I, Wilkowski D and Ducloy M 2016 *Opt. Lett.* **41** 2005–8
[12] Shibata K, Tojo S and Bloch D 2017 *Opt. Express* **25** 9476
[13] Le Kien F, Busch T, Truong V G and Chormaic S N 2017 *Phys. Rev.* A **96** 023835
[14] Le Kien F, Ray T, Nieddu T, Busch T and Chormaic S N 2018 *Phys. Rev.* A **97** 013821
[15] Ray T, Gupta R K, Gokhroo V, Everett J L, Nieddu T, Rajasree K S and Chormaic S N 2020 *New J. Phys.* **22** 062001
[16] Klimov V V and Ducloy M 2000 *Phys. Rev.* A **62** 043818
[17] Tojo S, Fujimoto T and Hasuo M 2005 *Phys. Rev.* A **71** 012507
[18] Barnett S M, Speirits F C and Babiker M 2022 *J. Phys. A: Math. Theor.* **55** 234008
[19] Berry M V 1998 Paraxial beams of spinning light *Proc. SPIE* **3487** 6–11
[20] Marcuse D 1989 *Light Transmission Optics* (Krieger)
[21] Snyder A W and Love J 2012 *Optical Waveguide Theory* (Springer Science & Business Media)
[22] Okamoto K 2006 *Fundamentals of Optical Waveguides* (Academic)
[23] Kapoor A and Singh G 2000 *J. Lightwave Technol.* **18** 849–52
[24] Sagué G, Baade A and Rauschenbeutel A 2008 *New J. Phys.* **10** 113008
[25] Frawley M C, Petcu-Colan A, Truong V G and Chormaic S N 2012 *Opt. Commun.* **285** 4648–54
[26] Kumar R, Gokhroo V, Deasy K, Maimaiti A, Frawley M C, Phelan C and Chormaic S N 2015 *New J. Phys.* **17** 013026
[27] Bougouffa S and Babiker M 2020 *Phys. Rev.* A **102** 063706
[28] Bougouffa S and Babiker M 2020 *Phys. Rev.* A **101** 043403
[29] Babiker M, Andrews D L and Lembessis V 2019 *J. Opt.* **21** 013001
[30] Lembessis V and Babiker M 2013 *Phys. Rev. Lett.* **110** 083002
[31] Al-Awfi S and Bougouffa S 2019 *Results Phys.* **12** 1357–62
[32] Bougouffa S 2021 *Results Phys.* **27** 104541
[33] Chan E A, Aljunid S A, Adamo G, Zheludev N I, Ducloy M and Wilkowski D 2019 *Phys. Rev.* A **99** 063801
[34] Sakai K, Yamamoto T and Sasaki K 2018 *Sci. Rep.* **8** 1–6

[35] Afanasev A, Carlson C E, Schmiegelow C T, Schulz J, Schmidt-Kaler F and Solyanik M 2018 *New J. Phys.* **20** 023032
[36] Le Kien F and Rauschenbeutel A 2014 *Phys. Rev.* A **90** 023805
[37] Petersen J, Volz J and Rauschenbeutel A 2014 *Science* **346** 67–71
[38] Lodahl P, Mahmoodian S, Stobbe S, Rauschenbeutel A, Schneeweiss P, Volz J, Pichler H and Zoller P 2017 *Nature* **541** 473–80
[39] Barnett S and Radmore P M 2002 *Methods in Theoretical Quantum Optics* vol 15 (Oxford University Press)
[40] Le Kien F, Busch T, Truong V G and Chormaic S N 2017 *Commun. Phys.* **27** 23–35